Available online at www.sciencedirect.com
SCIENCE DIRECT®
Journal of Sound and Vibration 268 (2003) 33–48
JOURNAL OF SOUND AND VIBRATION
www.elsevier.com/locate/jsvi

Non-stationary processes of rotor/bearing system in bifurcations

Q. Ding[a,*], A.Y.T. Leung[b]

[a] *Department of Mechanics, Tianjin University, Tianjin 300072, China*
[b] *Department of Building and Construction, City University of Hong Kong, Kowloon, Hong Kong*

Received 2 April 2002; accepted 4 November 2002

Abstract

Non-stationary processes of a rotor/bearing system were dealt with by taking the rotating angular speed, increases or decreases linearly at different levels of acceleration, as control parameter. The stationary bifurcation diagrams show that the period doubling bifurcation or quasi-periodic bifurcation, corresponding to the system with larger or smaller level of mass imbalance, respectively, occurs smoothly as the control parameter is increased or decreased in stationary manner. Then, the non-stationary processes of these two types of bifurcation were investigated by constructions of the non-stationary bifurcation diagrams using non-stationary bifurcation map technique. In the non-stationary bifurcation diagrams, penetrations can be easily observed during the forward and reverse transitions, and their absolute values increase with that of accelerations in all cases. Jumps exist only in forward period doubling transitions, which indicate the quick increases of the amplitudes of motion. Time flows and orbit trajectories are also presented to illustrate the non-stationary transition processes visually.

1. Introduction

Non-stationary processes occur naturally and widely in engineering field and physical world: in start-up and shut down of engines, in chemical and biochemical systems, in the movements of water, earth, air, etc. In stationary systems, all control parameters remain constant, whilst in non-stationary processes, one or more control parameters are time (process) dependent over extended ranges [1]. The early developments in non-stationary systems are attributed to two monographs

*Corresponding author. Tel.: +22-2740-8667.
E-mail address: qding@public.tpt.tj.cn (Q. Ding).

0022-460X/03/$ - see front matter © 2002 Elsevier Science Ltd. All rights reserved.
doi:10.1016/S0022-460X(02)01577-8

by Mitropolskii [1] and Evan-Iwanowski [2]. The recent achievements can be found in extensive publications [3–9]. Besides the characteristics of non-stationary processes of Duffing's oscillators which have been investigated over many years, some significant phenomena have also been revealed in recent years from actual complex systems, e.q. the shear deformable orthotropic plates, the laminated angle-ply column, a string with time-varying length and a mass–spring system attached at the lower end (a basic model of an elevator system), etc. The most typical phenomena existing in non-stationary processes are known as elimination of the discontinuities or jumps, though the transitions in stationary processes are smooth and penetration (delay or memory) together with anticipation, i.e., the transitions appear later or before compared to that in the stationary case as the concerned control parameter is varied in same direction. Bifurcation diagram is a useful tool to reveal visually the panorama of the non-stationary processes, including jumps, penetrations and anticipations, over extended parameter ranges. To overcome the shortage of the commonly used phase portraits or Poincaré maps, which give inadequate information because of the overlapping dynamical responses within ranges of time, the non-stationary bifurcation map (NBM) was suggested in Ref. [4] which determines the non-stationary bifurcation diagrams by recording the responses at the consecutive peaks of the forcing.

Non-stationary processes occur in rotor system in the stages of start-up and shut-down. But compared with the extensive studies on stationary processes, studies on non-stationary processes are rather limited. Recently, the non-stationary motions of rotor systems in rub events are reported. Yanabe et al. treated a rubbing problem when the unbalanced rotor is supported by springs and dampers and accelerated at a constant angular acceleration. The non-stationary rotor vibration due to collision with annular guard during passage through the critical speed is calculated. The result shows that the rotor cannot pass through the critical speed due to occurrence of backward whirl [10]. Ding and Chen investigated the partial differential equations governing the shaft/casing system with rubs using an explicit stable finite difference scheme. The result suggests that during passage through the first several critical speeds accelerated at a constant angular acceleration, the instability of the system can lead to the shaft's structural failure ultimately due to unlimited increase of the bending moments and stresses [11].

This paper deals with non-stationary processes of a rotor/bearing system. The rotating angular speed is taken as control parameter and increased or decreased linearly at different levels of angular acceleration. First, the stationary bifurcation diagrams are determined using the customary Poincaré maps. Then the non-stationary bifurcation diagrams are determined using the NBM technique. Some phenomena occurring in the processes of the non-stationary period-doubling transitions and the quasi-periodic transitions are uncovered in cases of positive and negative accelerations. Processes of transitions are revealed by presenting time flows and orbit trajectories.

2. Equation of motion

An isotropic flexible shaft attached with two imbalanced disks and supported at its two ends on lubricated bearings is considered (Fig. 1). The masses of disks 1 and 2 are m_1 and m_2 with eccentricity e_1 and e_2; the lumped masses at two ends of the shaft are m_3 and m_4, respectively. The

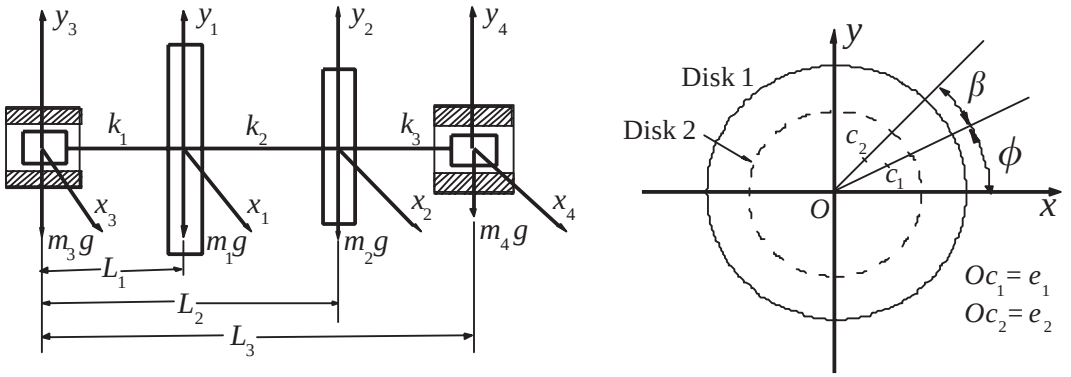

Fig. 1. Model of rotor/bearing system.

equivalent stiffnesses of the shaft in three spans are

$$k_1 = k_{11} + k_{12}, \quad k_2 = -k_{12}, \quad k_3 = k_{21} + k_{22}, \tag{1}$$

where k_{ij} $(i, j = 1, 2)$ are deduced from the simple beam theory:

$$k_{11} = 12\frac{L_2^2 L_3 EG}{L_1^2 \Lambda}, \quad k_{12} = k_{21} = -6\frac{(-L_1^2 + 2L_2L_3 - L_2^2)L_3 EG}{L_1(L_3 - L_2)\Lambda}, \quad k_{22} = 12\frac{(L_3 - L_1)^2 L_3 EG}{(L_3 - L_2^2)^2 \Lambda},$$
$$\Lambda = (L_1 - L_2)^2[4L_2L_3 - (L_1 + L_2)^2],$$

where E is Young's elastic modulus, and G the second moment of area of the cross-section of the shaft. Note that the effect that resulted from deviations of displacements from the plane vertical to shaft's axis are not included. Suppose bearings 3 and 4 are identical in size with parameters L, R and δ, the length, radius and mean radial clearance, respectively. μ is the viscosity of the lubricating oil; and f_{ix} and f_{iy} $(i = 3, 4)$ are the hydrodynamic forces generated in bearings 3 and 4 in x and y directions, respectively. The non-dimensional hydrodynamic forces are derived as

$$F_{ix} = \frac{f_{ix}}{\sigma W_i}, \quad F_{iy} = \frac{f_{iy}}{\sigma W_i}, \quad \sigma = \frac{\mu \Omega RL}{W_i}\left(\frac{R}{\delta}\right)^2\left(\frac{L}{2R}\right)^2, \quad W_i = m_i g, \quad i = 3, 4. \tag{2}$$

In non-stationary regime, starting from an initial angular velocity ω_0, the shaft is accelerated at a constant angular acceleration α. The rotational angle and the angular speed of the rotor can be expressed in the following form:

$$\phi = \tfrac{1}{2}\alpha t^2 + \omega_0 t, \quad \dot{\phi} = \Omega = \alpha t + \omega_0. \tag{3}$$

The equations of motion are deduced as

$$\begin{aligned}
\frac{W_1}{g}\ddot{x}_1 &= -k_1\left(x_1 - \tfrac{2}{3}x_3 - \tfrac{1}{3}x_4\right) - k_2\left(x_1 - \tfrac{1}{3}x_3 + \tfrac{1}{3}x_4 - x_2\right) + m_1e_1(\dot{\phi})^2\cos(\phi) + m_1e_1\alpha\sin(\phi),\\
\frac{W_1}{g}\ddot{y}_1 &= -k_1\left(y_1 - \tfrac{2}{3}y_3 - \tfrac{1}{3}y_4\right) - k_2\left(y_1 - \tfrac{1}{3}y_3 + \tfrac{1}{3}y_4 - y_2\right) - W_1 + m_1e_1(\dot{\phi})^2\sin(\phi) - m_1e_1\alpha\cos(\phi),\\
\frac{W_2}{g}\ddot{x}_2 &= -k_2\left(x_2 + \tfrac{1}{3}x_3 - \tfrac{1}{3}x_4 - x_1\right) - k_3\left(x_2 - \tfrac{1}{3}x_3 - \tfrac{2}{3}x_4\right) + m_2e_2(\dot{\phi})^2\cos(\phi+\beta) + m_2e_2\alpha\sin(\phi+\beta),\\
\frac{W_2}{g}\ddot{y}_2 &= -k_2\left(y_2 + \tfrac{1}{3}y_3 - \tfrac{1}{3}y_4 - y_1\right) - k_3\left(y_2 - \tfrac{1}{3}y_3 - \tfrac{2}{3}y_4\right) - W_2 + m_2e_2(\dot{\phi})^2\sin(\phi+\beta) - m_2e_2\alpha\cos(\phi+\beta),\\
\frac{W_3}{g}\ddot{x}_3 &= k_1\left(x_1 - \tfrac{2}{3}x_3 - \tfrac{1}{3}x_4\right) + f_{3x},\\
\frac{W_3}{g}\ddot{y}_3 &= k_1\left(y_1 - \tfrac{2}{3}y_3 - \tfrac{1}{3}y_4\right) - W_3 + f_{3y},\\
\frac{W_4}{g}\ddot{x}_4 &= k_3\left(x_2 - \tfrac{1}{3}x_3 - \tfrac{2}{3}x_4\right) + f_{4x},\\
\frac{W_4}{g}\ddot{y}_4 &= k_3\left(y_2 - \tfrac{1}{3}y_3 - \tfrac{2}{3}y_4\right) - W_4 + f_{4y},
\end{aligned} \tag{4}$$

where $W_i = m_i g, \quad i = 1, 2.$

Introducing the following non-dimensional quantities:

$$\tau = \sqrt{\frac{k_{11}}{m_1}}t = \gamma t, \quad X_i = \frac{x_i}{\delta}, \quad Y_i = \frac{y_i}{\delta}, \quad \bar{m}_i = \frac{m_1}{m_i}, \quad i = 1,2,3,4, \quad \bar{e}_i = \frac{e_i}{\delta}, \quad i = 1,2,$$

$$\bar{k}_i = \frac{k_i}{k_{11}}, \quad i = 1,2,3, \quad \bar{\omega}_0 = \frac{\omega_0}{\gamma}, \quad \bar{\alpha} = \frac{\alpha}{\gamma^2}, \quad \bar{g} = \frac{g}{\delta\gamma^2}.$$

Eq. (4) are then rewritten in the following dimensionless form:

$$\begin{aligned}
X_1'' &= -\bar{k}_1(X_1 - \tfrac{2}{3}X_3 - \tfrac{1}{3}X_4) - \bar{k}_2(X_1 - \tfrac{1}{3}X_3 + \tfrac{1}{3}X_4 - X_2) + \bar{e}_1(\phi')^2\cos(\phi) + \bar{e}_1\bar{\alpha}\sin(\phi),\\
Y_1'' &= -\bar{k}_1(Y_1 - \tfrac{2}{3}Y_3 - \tfrac{1}{3}Y_4) - \bar{k}_2(Y_1 - \tfrac{1}{3}Y_3 + \tfrac{1}{3}Y_4 - Y_2) - \bar{g} + \bar{e}_1(\phi')^2\sin(\phi) - \bar{e}_1\bar{\alpha}\cos(\phi),\\
X_2'' &= -\bar{k}_2\bar{m}_2(X_2 + \tfrac{1}{3}X_3 - \tfrac{1}{3}X_4 - X_1) - \bar{k}_3\bar{m}_2(X_2 - \tfrac{1}{3}X_3 - \tfrac{2}{3}X_4) + \bar{e}_2(\phi')^2\cos(\phi+\beta) + \bar{e}_2\bar{\alpha}\sin(\phi+\beta),\\
Y_2'' &= -\bar{k}_2\bar{m}_2(Y_2 + \tfrac{1}{3}Y_3 - \tfrac{1}{3}Y_4 - Y_1) - \bar{k}_3\bar{m}_2(Y_2 - \tfrac{1}{3}Y_3 - \tfrac{2}{3}Y_4) - \bar{g} + \bar{e}_2(\phi')^2\sin(\phi+\beta) - \bar{e}_2\bar{\alpha}\cos(\phi+\beta),\\
X_3'' &= \bar{k}_1\bar{m}_3(X_1 - \tfrac{2}{3}X_3 - \tfrac{1}{3}X_4) + \sigma\bar{g}F_{3X},\\
Y_3'' &= \bar{k}_1\bar{m}_3(Y_1 - \tfrac{2}{3}Y_3 - \tfrac{1}{3}Y_4) - \bar{g} + \sigma\bar{g}F_{3Y},\\
X_4'' &= \bar{k}_3\bar{m}_4(X_2 - \tfrac{1}{3}X_3 - \tfrac{2}{3}X_4) + \sigma\bar{g}F_{4X},\\
Y_3'' &= \bar{k}_3\bar{m}_4(Y_2 - \tfrac{1}{3}Y_3 - \tfrac{2}{3}Y_4) - \bar{g} + \sigma\bar{g}F_{4Y},
\end{aligned} \tag{5}$$

where $(\,)' = \mathrm{d}(\,)/\mathrm{d}\tau$. $\phi = \frac{1}{2}\bar{\alpha}\tau^2 + \bar{\omega}_0\tau$, $\phi' = \bar{\alpha}\tau + \bar{\omega}_0$. Instead of the steady "π" or "2π" film cavitation model, Zhang et al adopted the zero-upper and -lower boundary conditions, i.e., the free boundaries of the outline of oil film were determined at the points with zero pressure, in

deducing a non-steady non-linear hydrodynamic forces generated by oil film [12]. For short bearing, the non-dimensional hydrodynamic forces F_{iX}, F_{iY} ($i=3,4$) are calculated by the analytical model as stated in the Appendix.

The following values of realistic physical parameters are used in numerical simulation: $m_1=1.0\,\text{kg}$, $m_2=0.6\,\text{kg}$, $m_3=m_4=0.2\,\text{kg}$, $L_3=3L_1=\frac{3}{2}L_2=0.8\,\text{m}$, $d=0.011\,\text{m}$ (diameter of the shaft), $E=200\,\text{GPa}$; $R=12.5\,\text{mm}$, $L=16\,\text{mm}$, $\delta=0.25\,\text{mm}$, $\mu=0.0373\,\text{N s/m}^2$.

3. Stationary bifurcations

Stability analysis shows that the perfectly balanced system (5) (i.e., $\bar{e}_i=0$, $i=1, 2$), loses its stability through Hopf bifurcation. Analyzing the eigenvalues of the linearized perturbation system at static equilibrium position can result in threshold speed and dimensionless whirl frequency [13]. For the mass imbalanced system (5) (i.e., $\bar{e}_1\neq 0$ and/or $\bar{e}_2\neq 0$), behaviour of the periodically perturbed Hopf bifurcation depends on the level of mass imbalance. Generally, smaller level of mass imbalance yields quasi-period bifurcation, whilst larger level of mass imbalance yields period doubling bifurcation.

Letting $\alpha=0$ and applying Runge–Kutta–Fehlerg integration to solve Eq. (5), bifurcation diagrams are obtained using the brute-force algorithm [14] as the control parameter, the rotational angular speed of the rotor, increases or decreases in a stationary manner as shown in Figs. 2 and 3.

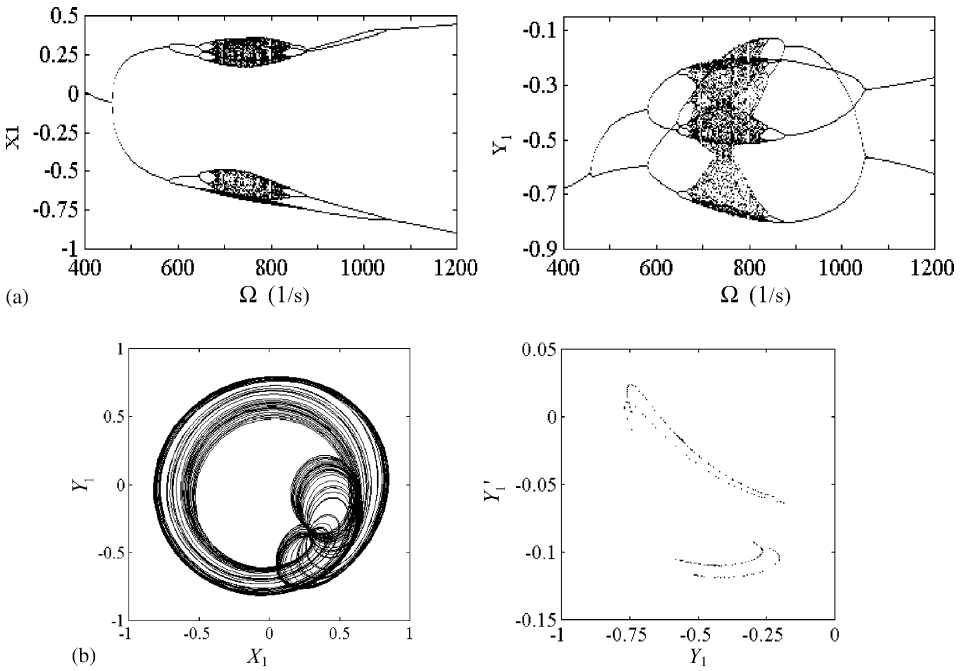

Fig. 2. Stationary period-doubling bifurcation ($\bar{e}_1=\bar{e}_2=0.4$ and $\beta=\pi/6$): (a) bifurcation diagrams with varying angular speed, (b) orbit trajectory and Poincaré map ($\Omega=550\,\text{s}^{-1}$).

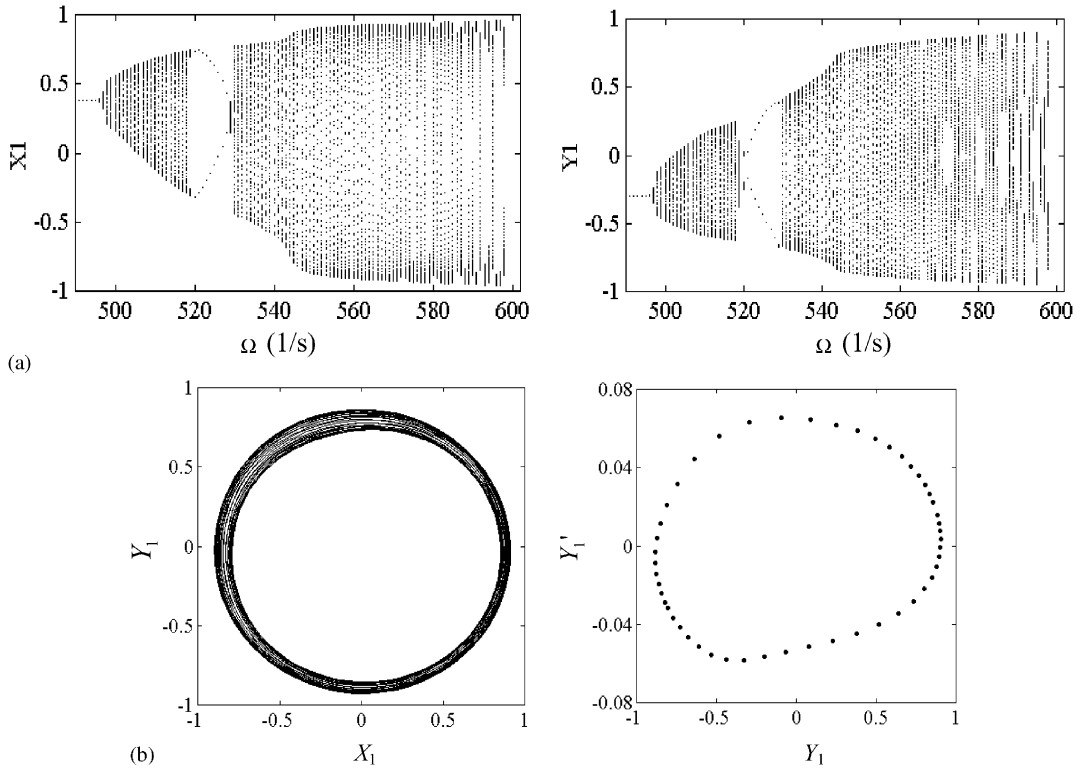

Fig. 3. Stationary quasi-periodic bifurcation ($\bar{e}_1 = 0.01$, $\bar{e}_2 = 0.02$ and $\beta = \pi/3$): (a) bifurcation diagrams with varying angular speed, (b) orbit trajectory and Poincaré map($\Omega = 550\,\mathrm{s}^{-1}$).

For the rotor with larger level of mass imbalance ($\bar{e}_1 = \bar{e}_2 = 0.4$ and $\beta = \pi/6$) a sequence of forward period doubling bifurcations leads the system enter into chaotic regime (see Fig. 2(b)), and then it experiences a sequence of reverse period doubling bifurcations. All the forward and reverse transitions of motion are smooth in bifurcation diagrams. The rotor enters into a limit periodic motion, i.e., there no further qualitative change in the state of motion as the control parameter varies further [1] with period 2 when speeding up and return back to one with period 1 when speeding down. The periodic motion with period 2^n ($n = 0, 1, 2, 3, \ldots$) is referred as 2^nP motion or simply 2^nP in the following. The transition from $2^{n-1}P$ to 2^nP, or from 2^nP to $2^{n-1}P$, occurs smoothly as the control parameter arrives at a critical speed, which is referred in the following as bifurcation or transition speed. For example, the transition speeds of $2P$ to $4P$ (before the chaotic regime) and $4P$ to $2P$ (after the chaotic regime) are 580 and $1050\,\mathrm{s}^{-1}$, respectively, as the rotor speeds up. Conversely they are 1050 and $580\,\mathrm{s}^{-1}$, respectively, as the rotor slowly down (see Table 1).

For the rotor with smaller level of mass imbalance ($\bar{e}_1 = 0.01$, $\bar{e}_2 = 0.02$ and $\beta = \pi/3$), the transition from P motion to quasi-periodic motion (referred as QP motion or QP later) or from QP motion to P motion when the rotor speeds up or down, respectively, occurs at the transition speed $495\,\mathrm{s}^{-1}$. The QP motion lasts over a broad range of the control parameter and settles down gradually to a motion which occupies the full inside space of bearing, with a slow whirling speed.

Table 1
Transition speeds (s^{-1}) of the stationary and nonstationary period doubling bifurcations, and corresponding penetration values (s^{-1})

α (s^{-2})	Transitions (bifurcations) of motion					
	$P \Leftrightarrow 2P$	$2P \Leftrightarrow 4P$	$4P \Leftrightarrow 8P$	Chaotic regime	$8P \Leftrightarrow 4P$	$4P \Leftrightarrow 2P$
0 (Stationary)	460	580	642	—	875	1050
12	472(12)	599(19)	657(15)	—	882(7)	1057(7)
−12	446(−14)	572(−8)	637(−5)	—	860(−15)	1012(−38)
24	480(20)	608(28)	670(28)	—	884(9)	1061(11)
−24	438(−22)	565(−15)	634(−8)	—	850(−25)	1000(−50)
48	487(27)	626(46)	*	—	885(10)	1066(16)
−48	432(−28)	564(−16)	630(−12)	—	*	973(−77)

Annotation: Transitions: from left to right for $\alpha > 0$, and from right to left for $\alpha < 0$; numbers among the parentheses are corresponding penetration values.
*Represents that the transition speed is hardly to be determined.

One can easily find a "window" of $2P$ among the QP motion regime over the Ω range of 520 – 529. It is actually the subharmonic resonance with order 1/2. Such a phenomenon is referred as "mode-locking", which often occurs in the dynamical systems with strong, especially non-smooth, non-linearity [15].

4. Non-stationary bifurcations

4.1. Non-stationary bifurcation map

On the basis of the NBM [4] and in consideration of the characteristic of the mass imbalanced excitation, we define the non-stationary maps by recording the responses X and Y of Eq. (5) at consecutive peaks of normal inertial imbalance force of disk 1 projected in positive X direction, i.e., at the time τ_N resulting from the maxima of the function $\cos(\frac{1}{2}\bar{\alpha}\tau^2 + \bar{\omega}_0\tau)$:

$$\tau_N = \frac{\bar{\omega}_0}{\bar{\alpha}}\left(\sqrt{(1 + 4\pi N\bar{\alpha}/\bar{\omega}_0^2)} - 1\right), \quad N = 0, 1, 2, \ldots, \tag{6}$$

where N denotes the number of evolution cycles. Note that the non-stationary maps can be presented in terms of N, τ_N or $\Omega(\tau_N)$, respectively. For stationary case with $\bar{\alpha} = 0$, the mapping points used to construct bifurcation diagram, for any concerned value of the control parameter, are obtained at the consecutive sections of time $\tau_N = N \times 2\pi/\bar{\omega}_0$ when the motion is in steady state (after transient process). The number of mapping points must be larger than the period number of current periodic motion or large enough for current non-periodic motion (such as the quasi-periodic or chaotic ones). For example, projecting the points in Poincaré map on the Y_1-axis (Fig. 3(b)), one gets the mapping points in bifurcation diagram $\Omega - Y_1$ corresponding to $\Omega = 550\,s^{-1}$, see Fig. 3(a), whereas for non-stationary case with $\bar{\alpha} \neq 0$, only one mapping point will be obtained for any concerned value of the control parameters, i.e., N, τ_N or $\Omega(\tau_N)$. So the construction of non-stationary bifurcation diagrams on the basis of such non-stationary maps

allow us to identify the individual types of dynamical responses (periodic, quasi-periodic and chaos) and their ranges in terms of control parameters of interest. It offers considerable advantages over the commonly used phase portrait or Poincaré maps in that the latter two may present inadequate information by the overlapping of various types, or even the same type, dynamical responses within the ranges of time.

4.2. Non-stationary period doubling bifurcations

For the case $\bar{e}_1 = \bar{e}_2 = 0.4$ and $\beta = \pi/6$, the non-stationary period doubling bifurcations (transitions) occur as the rotor speeds up or down at a certain level of acceleration. That is after experiencing a sequence of successive transitions from $2^{n-1}P$ to 2^nP, the system enters into chaotic regime and then experiences a sequence of reverse successive transitions from 2^nP to $2^{n-1}P$, as shown in Fig. 4 ($\alpha = 24$ and $-24\,s^{-2}$). Comparing to stationary case, the non-stationary period doubling bifurcation has following characteristics:

(1) There are obvious jumps in bifurcation diagrams during forward transitions. In other words, the transition from the periodic motion with smaller period number to that with larger period number, i.e., $2^{n-1}P$ to 2^nP, are non-smooth, whereas the reverse bifurcation processes, i.e., 2^nP to $2^{n-1}P$, are smooth.

(2) Penetration is defined as the difference between the control parameter values at which the stationary and non-stationary transitions of same order occur [3]. For the concerned rotor/bearing system, it is the difference between the stationary and non-stationary transition speeds of the same order of bifurcation. Calculations show that there exist penetrations in both forward and reverse transitions, and penetration value increases with the value of acceleration (both values are absolute whenever they are concerned hereafter). Taking $\alpha = 12$, 24 and $48\,s^{-2}$ for example, the penetration values are 12, 20 and $27\,s^{-1}$) for transition P to $2P$, and 7, 11 and $16\,s^{-1}$ for $4P$ to $2P$. For $\alpha = -12$, -24 and $-48\,s^{-2}$, they are -38, -50 and $-77\,s^{-1}$, respectively, for transition $2P$ to $4P$. More details can be found in Table 1. This fact suggests that the penetration phenomena can reasonably be owed to the rotational inertia effect. Subsequently, the jumps in bifurcation diagrams during forward transitions can also be owed to penetrations. Comparably, the penetration values in forward transitions are generally larger than that in reverse transitions.

(3) Due to penetrations, the existing ranges of periodic motions on control parameter axis are compressed to zero quickly as the period number increases in forward transitions. For example, the transition speed of $4P$ to $8P$ for $\alpha = 48\,s^{-2}$ can hardly be determined. In fact, the motion is nearly in chaotic regime just after occurrence of transition $2P$ to $4P$. Because the penetration values in forward transitions are generally much larger than that in reverse transitions, the existing range of chaotic motion is also compressed narrower and narrower with increase of α.

Details of non-stationary period doubling transitions, P to $2P$ to $4P$ to chaos to $4P$ to $2P$, are revealed by the time flows and the orbit trajectories in (X_1, Y_1) plane as presented in Fig. 5. One finds that so-called "periodic motions" in non-stationary process are only similar to those in stationary process. For example, orbit trajectory of the non-stationary P motion is a nearly but never a closed circle. In addition, orbit trajectory is always smooth during any transition. So the jumps in bifurcation diagrams indicate only the quick increase of the amplitude of motion. Obviously, the amplitude of the motion increases monotonically with the successive appearances of the forward and reverse transitions as Ω is increased.

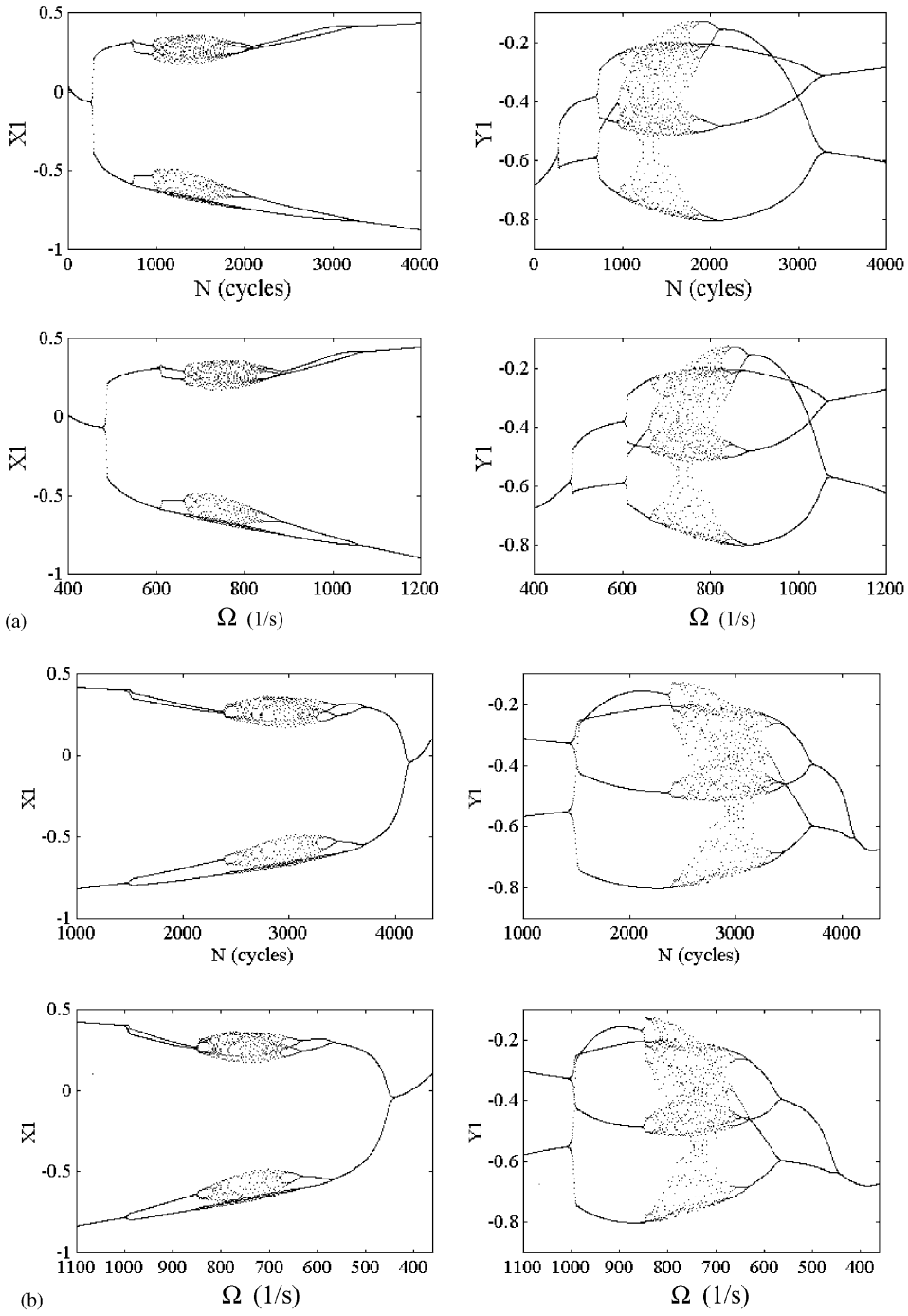

Fig. 4. Non-stationary period doubling bifurcation diagrams with varying cycle and angular speed ($\bar{e}_1 = 0.4$, $\bar{e}_2 = 0.4$ and $\beta = \pi/6$): (a) $\alpha = 24\,\mathrm{s}^{-2}$ and $\omega_0 = 360\,\mathrm{s}^{-1}$ (b) $\alpha = -24\,\mathrm{s}^{-2}$ and $\omega_0 = 1200\,\mathrm{s}^{-1}$.

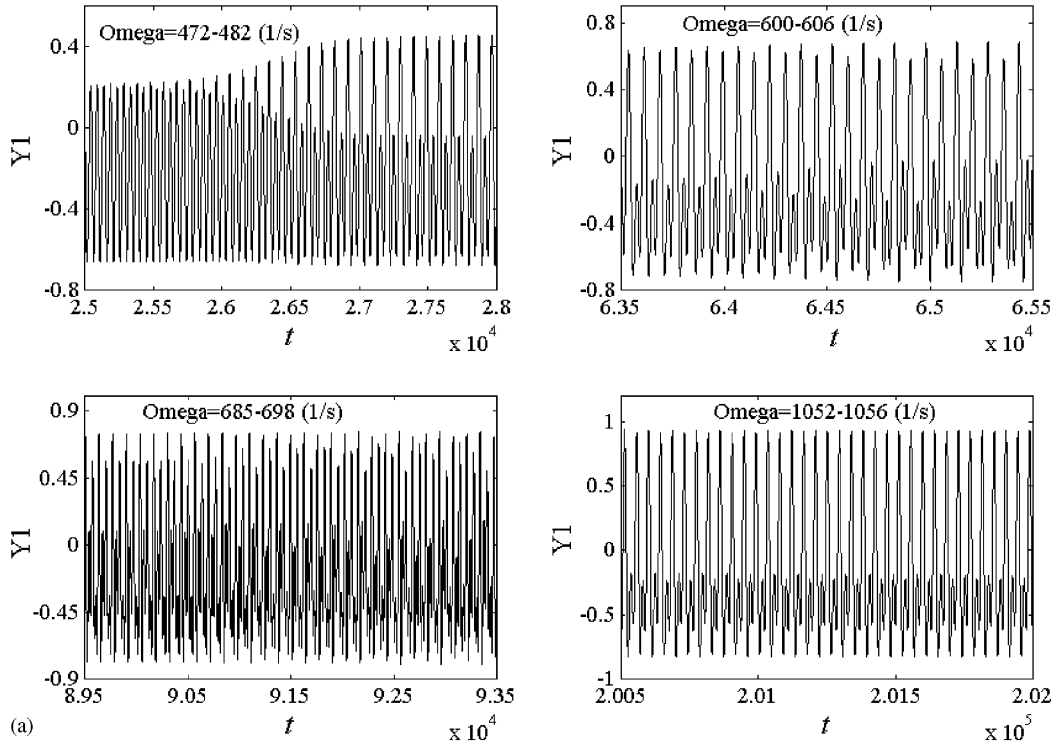

Fig. 5. Transitions from P to $2P$; $2P$ to 4P; $4P$ to Chaos; and $4P$ to 2P. ($\bar{e}_1 = 0.4$, $\bar{e}_2 = 0.4$ and $\beta = \pi/6$; $\omega_0 = 360\ \mathrm{s}^{-1}$ and $\alpha = 12\ \mathrm{s}^{-2}$): (a) Time flows (Omega $= \Omega$); (b) orbit trajectories in plane (X_1, Y_1).

4.3. Non-stationary quasi-periodic bifurcations

For the case $\bar{e}_1 = 0.01$, $\bar{e}_2 = 0.02$ and $\beta = \pi/3$, non-stationary quasi-periodic motion bifurcates from P motion as the rotor speeds up, whereas the quasi-periodic motion transits to P motion as the rotor speeds down, as shown in Fig. 6 ($\alpha = 24$ and $-24\ \mathrm{s}^{-2}$). The non-stationary quasi-periodic bifurcation diagrams look very different from the stationary ones. The reason is that in construction of the non-stationary diagram, only one, rather than many, mapping point was employed for any concerned value of the control parameter, as already mentioned in Section 4.1. As well known, there are two basic frequency components in QP motion. One is the rotating frequency of the rotor, which represents the forced vibration of the system induced by the mass imbalance. Another one with lower value represents the self-excited vibration after occurrence of bifurcation. It makes the non-stationary bifurcation diagram look like that of period 2 motion. But as the ratio of the values of these two frequencies is irrational, the motion synthesized by them is only the "almost-periodic" or "quasi-periodic". It makes the non-stationary bifurcation diagram appear like contour line of time flow of a vibration response with "beating" behaviour with varying control parameter. The length of a section of beating in time axis is what has been referred a "quasi-period" of the QP. The difference in appearances between the QP motion and

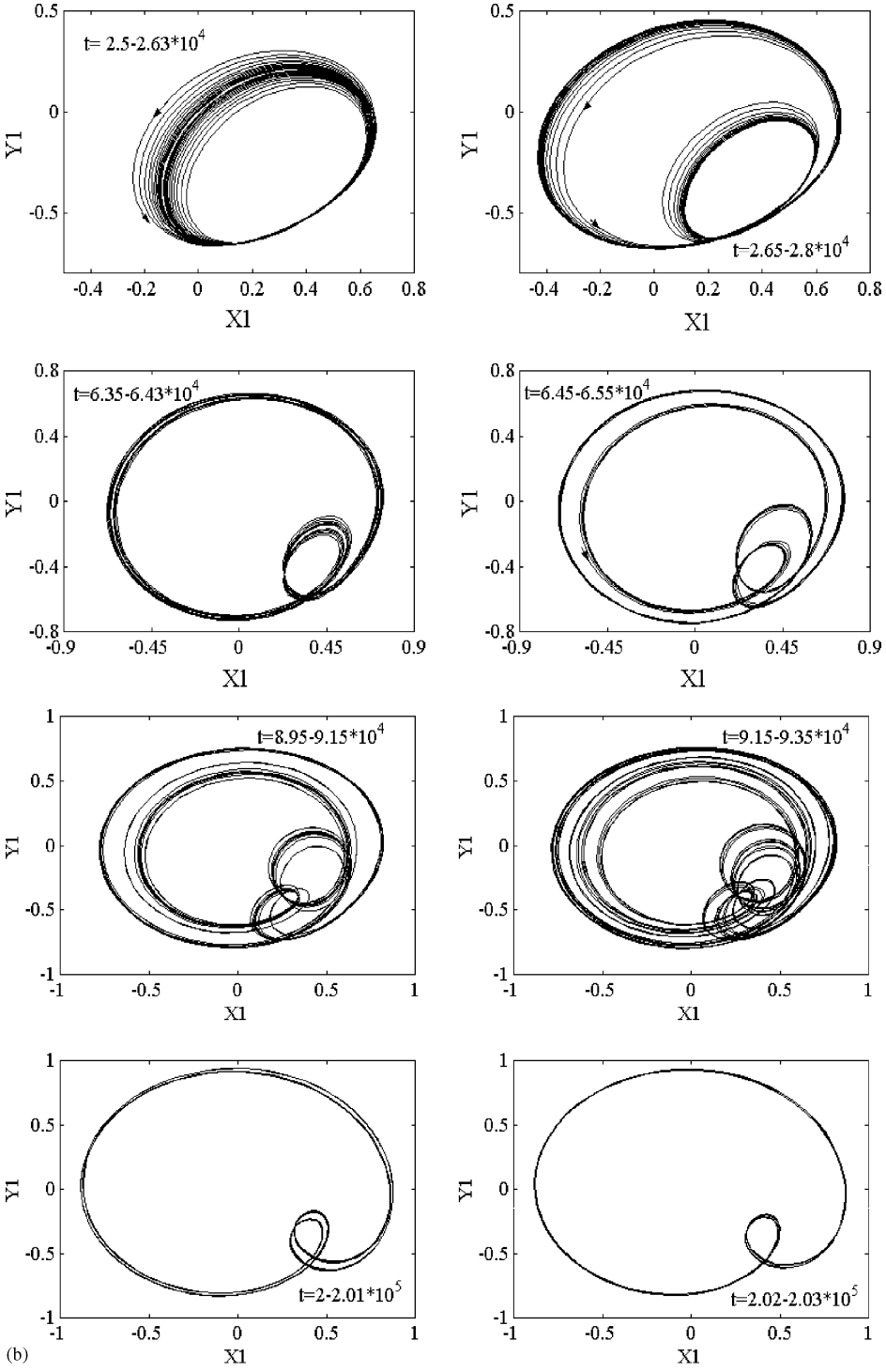

Fig. 5 (*continued*).

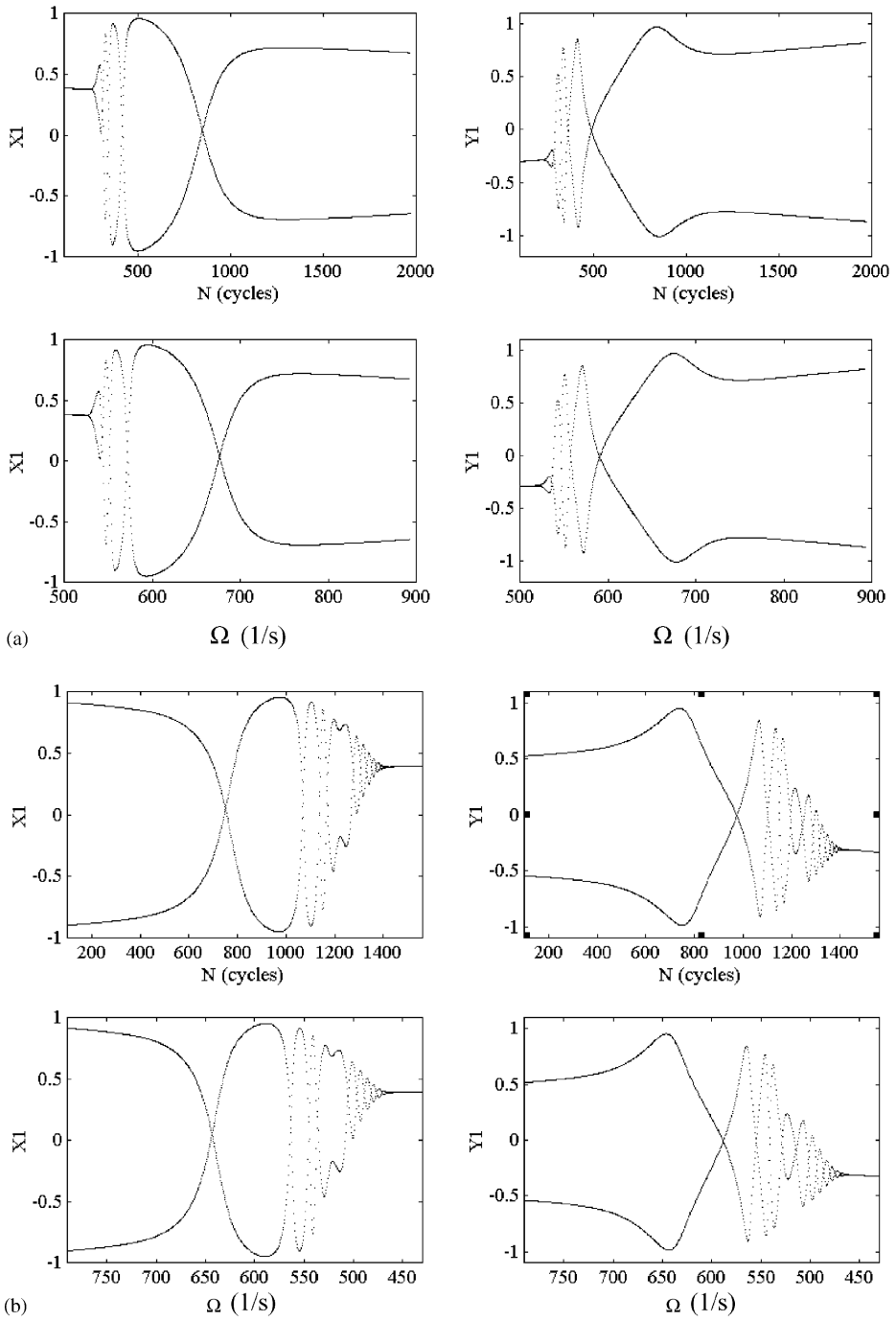

Fig. 6. Non-stationary bifurcation diagrams with varying cycle and angular speed ($\bar{e}_1 = 0.01, \bar{e}_2 = 0.02$ and $\beta = \pi/3$): (a) $\omega_0 = 460\ (s^{-1})$ and $\alpha = 24\ (s^{-2})$ (b) $\omega_0 = 800\,s^{-1}$ and $\alpha = -24\,s^{-2}$.

chaotic motion, for the latter there is no such a basic "quasi-period" as the former, is also much larger in non-stationary case than that in stationary case, see Figs. 6 and 4 for comparison.

Fig. 7 gives details of non-stationary transitions from P to QP and from QP to P, by time flows and orbit trajectories in $(X_1,\ Y_1)$ plane. The characteristics of the non-stationary quasi-periodic bifurcations are listed in the following:

(1) There is no jump in both forward, P to QP, and reverse, QP to P, transitions. Nevertheless, the increase of amplitude of motion after P to QP transition in non-stationary case is still much faster than that in stationary case.

(2) Penetrations exist in both the forward and reverse transitions. Note that the stationary transition speed is $495\,s^{-1}$. The penetration values increase with that of acceleration. For example, the transition speeds and corresponding penetration values of P to QP are 525/30, 528/33 and $531/36\,s^{-1}$ for $\alpha = 12$, 24 and $48\,s^{-2}$, respectively, whereas the transition speeds and corresponding penetration values of QP to P are $472/-23$, $455/-40$ and $436/-59\,s^{-1}$, for $\alpha = -12$, -24 and $-48\,s^{-2}$, respectively. The penetration value of QP to P transition is larger and increases faster than that of P to QP transition as the acceleration increases. The reason is that comparing to the smaller forced vibration component, resulting from the small level of mass imbalance, the self-excited whirling component is predominant in QP motion and has strong ability to keep this type of motion owing to the whirling inertia effect.

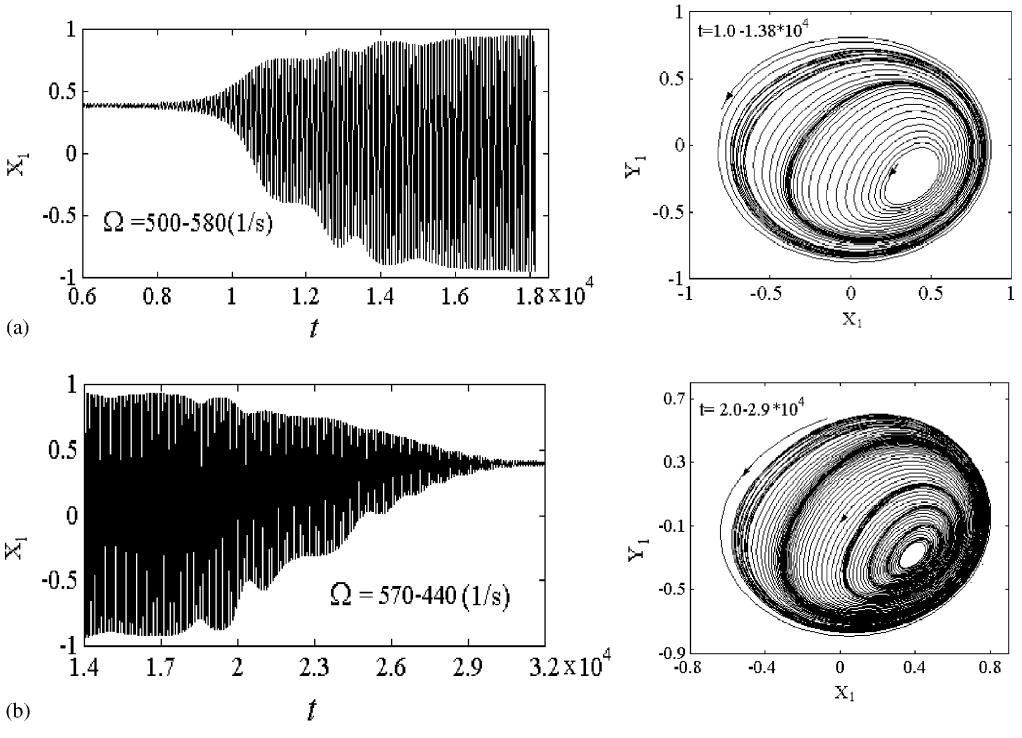

Fig. 7. Non-stationary transitions from P to QP and QP to P ($\bar{e}_1 = 0.01$, $\bar{e}_2 = 0.02$ and $\beta = \pi/3$): (a) $\omega_0 = 460\ s^{-1}$ and $\alpha = 24\ s^{-2}$ (b) $\omega_0 = 670\ s^{-1}$ and $\alpha = -24\ s^{-2}$.

(3) The limit motion of non-stationary quasi-periodic transitions as the rotor speeds up is also a half-frequency whirling (or whip) in the full space inside the bearings. Fig. 7 shows that its orbit trajectory looks like a P motion because the self-excited vibration component is in predominance. When the rotor speeds down, more "beatings" will be experienced before transiting from QP to P.

5. Conclusions

The non-stationary processes can be effectively revealed using non-stationary bifurcation diagrams, constructed on basis of the NBM, in terms of both the number of evolution cycle and rotating angular speed. The non-stationary period doubling transitions include forward transitions (from $2^{n-1}P$ to 2^nP), chaotic regime and reverse transitions (from $2^{n-1}P$ to 2^nP), whether the rotor speeds up or down. The limit periodic motions with periods 2 and 1 correspond to speeding up and down. Penetrations exist in both forward and reverse transition processes, with an increasing absolute value with that of acceleration. Penetrations in forward transitions bring jumps in non-stationary bifurcation diagrams, which indicate the rapid increases of the amplitudes of responses. Penetrations exist also in non-stationary transitions, from periodic motion to quasi-periodic motion, as the rotor speeds up and the reverse one occurs as the rotor speeds down. Because the self-excited whirling component is predominant in quasi-periodic motion and has strong ability, owed to the whirling inertia effect, to keep such a state of motion, penetration of the latter transition is more obvious than that of the former transition. In addition, though there is no jump, the amplitude of quasi-periodic response in non-stationary case increases much faster as the speed increases, after occurrence of the forward transitions, than that in stationary case.

In engineering, the transition from P to quasi-periodic motion or P to $2P$ motion is referred as occurrence of oil whirl/whip, or lower-frequency vibration of the rotor/bearing systems. It is unfavourable to the safe operations. Not like the effective application to avoid the failure in passage through the critical speed due to occurrence of backward whirl from the rub events, speeding up in a certain level of acceleration could only delay but not avoid the occurrences of oil whirl/whip. What is worse, the rapidly increase of amplitude of response after occurrences of oil whirl/whip brings more violent and harmful vibration to the system.

Acknowledgements

This research was supported by the NNSF of China under Grant No. 10272078.

Appendix A. Expression of the non-dimensional hydrodynamic force ($i = 3, 4$)

$$\begin{bmatrix} F_{iX} \\ F_{iY} \end{bmatrix} = -\frac{C}{\phi'}\begin{bmatrix} X_i' \\ Y_i' \end{bmatrix} - K\begin{bmatrix} X_i \\ Y_i \end{bmatrix}, \quad C = \begin{bmatrix} c_{11} & c_{12} \\ c_{21} & c_{22} \end{bmatrix}, \quad K = \frac{1}{2}\begin{bmatrix} -C_2 & C_3 \\ -C_3 & -C_2 \end{bmatrix},$$

$$c_{11} = C_1\cos^2\varphi + C_3\sin^2\varphi - C_2\sin 2\varphi, \quad c_{22} = C_1\sin^2\varphi + C_3\cos^2\varphi + C_2\sin 2\varphi,$$

$$c_{12} = c_{21} = C_2(\cos^2\varphi - \sin^2\varphi) + \tfrac{1}{2}(C_1 - C_3)\sin 2\varphi,$$

$$C_1 = \frac{4\varepsilon\varepsilon' A\left[3A^2 + (2-5\varepsilon^2)\varepsilon^2\left(\Phi' - \tfrac{1}{2}\right)^2\right]}{(1-\varepsilon^2)^2\left[A^2 - \varepsilon^4\left(\Phi' - \tfrac{1}{2}\right)^2\right]^2} + \frac{2+4\varepsilon^2}{(1-\varepsilon^2)^{5/2}}\Delta\varphi,$$

$$C_2 = \frac{8\varepsilon^4 A\left(\Phi' - \tfrac{1}{2}\right)^3}{\left[A^2 - \varepsilon^4\left(\Phi' - \tfrac{1}{2}\right)^2\right]^2},$$

$$C_3 = \frac{4\varepsilon\varepsilon' A\left[A^2 + (\varepsilon^3 - 2)\varepsilon^2\left(\Phi' - \tfrac{1}{2}\right)^2\right]}{(1-\varepsilon^2)\left[A^2 - \varepsilon^4\left(\Phi' - \tfrac{1}{2}\right)^2\right]^2} + \frac{2}{(1-\varepsilon^2)^{3/2}}\Delta\varphi,$$

$$A = \sqrt{\varepsilon'^2 + \left(\Phi' - \tfrac{1}{2}\right)^2\varepsilon^2}, \quad \Delta\varphi = \pi + 2\tan^{-1}\left(\frac{\varepsilon\varepsilon'}{A(1-\varepsilon^2)^{1/2}}\right),$$

where

$$\varepsilon = \sqrt{X_i^2 + Y_i^2}, \quad \varepsilon' = \frac{X_i X_i' + Y_i Y_i'}{\varepsilon\phi'}, \quad \Phi' = \frac{X_i Y_i' - Y_i X_i'}{\varepsilon^2\phi'}, \quad \cos\varphi = \frac{X_i}{\varepsilon}.$$

References

[1] Y.Y. Mitropolskii, Problems of The Asymptotic Theory of Non-stationary Vibrations, Daniel Davey Press, New York, 1965.

[2] R.M. Evan-Iwanowski, Resonance Oscillations in Mechanical Systems, Elsevier, Amsterdam, 1976.

[3] C.–H. Lu, R.M. Evan-Iwanowski, Periodic doubling bifurcation problems in the softening Duffing oscillator with non-stationary excitation, Nonlinear Dynamics 5 (1994) 401–402.

[4] R.M. Evan-Iwanowski, C.–H. Lu, Non-stationary process: non-stationary bifurcation maps, evolutionary dynamics, Nonlinear Dynamics 21 (2000) 337–352.

[5] F.A. Moslehy, R.M. Evan-Iwanowski, The effect of non-stationary processes on chaotic and regular responses of the Duffing oscillator, International Journal of Nonlinear Mechanics 26 (1991) 61–71.

[6] A. Nayfeh, K.R. Asfar, Non-stationary parametric oscillation, Journal of Sound and Vibration 124 (1988) 529–537.

[7] C.–H. Lu, R.M. Evan-Iwanowski, H.Y. Jia, On the stabilizaton of non-stationary parametric main resonance of a laminated angle-ply column, International Journal of Computers and Structures 61 (1996) 695–704.

[8] C.–H. Lu, R. Mao, R.M. Evan-Iwanowski, Non-stationary parametric responces of shear deformable orthotropic plates, Journal of Sound and Vibration 184 (1995) 329–342.

[9] Y. Terumichi, M. Ohtsuka, M. Yoshizawa, Y. Fukawa, Y. Tsujioka, Non-stationary vibrations of a string with time-varying length and a mass-spring system attached at the lower end, Nonlinear Dynamics 12 (1997) 39–55.

[10] S. Yanabe, Y. Kaneko, N. Kanemitsu, N. Tomi, K. Sugiyama, Rotor vibration due to collision with annular guard during passage through critical speed, Journal of Vibration and Acoustics, Transactions of the American Society of Mechanical Engineers 120 (1998) 544–550.

[11] Q. Ding, Y.S. Chen, Non-stationary motion and instability of a shaft/casing system with rubs, Journal of Vibration and Control 7 (2001) 327–338.

[12] W. Zhang, Ageneral mathematical model of nonlinear non-steady oil film force in dynamic load bearing, in: D.J. Wang, G.J. Qu (Eds.), Advances in Engineering Mechanics, Peking University Press, Beijing, 1998, pp. 158–167.
[13] Q. Ding, J.E. Cooper, A.Y.T. Leung, Hopf bifurcation analysis of a rotor/seal system, Journal of Sound and Vibration 252 (2002) 817–833.
[14] T.S. Parker, L.O. Chua, Practical Numerical Algorithms for Chaotic Systems, Springer, New York, 1989.
[15] Q. Ding, A.Y.T. Leung, J.E. Cooper, Dynamic analysis of a self-excited hysteretic system, Journal of Sound and Vibration 245 (2001) 151–164.